Atomic-Layer- and Crystal-Orientation-Resolved $3d_{5/2}$ Binding Energy Shift of Ru(0001) and Ru($10\bar{1}0$) Surfaces

Yan Wang,[†] Yanguang Nie,[‡] Lingling Wang,[†] and Chang Q. Sun*[,‡]

School of Physics and Microelectronics Science, Hunan University, Changsha 410082, China, and School of Electrical & Electronic Engineering, Nanyang Technological University, Singapore 639798, Singapore

Received: October 6, 2009; Revised Manuscript Received: November 11, 2009

Theoretical reproduction of the Ru(0001) and Ru($10\bar{1}0$) surface XPS profiles has led to the following information: (i) the $3d_{5/2}$ energy level of an isolated Ru atom ($E_{3d}(z = 0) = 275.883 \pm 0.002$ eV); (ii) the energy shift of the $3d_{5/2}$ energy ($\Delta E_{3d}(z = 12) = 3.661$ eV) from the $E_{3d}(0)$ upon bulk formation; (iii) the effective z values of the surface sublayers; (iv) the coordination (z) dependence of the energy shift: $E_{3d}(z) = \langle E_{3d}(0)\rangle + \Delta E_{3d}(12)c_z^{-1} = 275.883 \pm 0.002 + 3.661/c_z$ (eV), with $c_z = 2/\{1 + \exp[(12 - z)/(8z)]\}$ being the z-dependent bond contraction coefficient; (v) the z-dependent lattice strain, binding energy density gain, and atomic cohesive energy remnant in the surface layers; and importantly, (vi) the physical origin for the surface-induced positive core-level shift. It has been clarified that the binding energy shift arises from the perturbation in the Hamiltonian by the shorter and stronger bonds between undercoordinated atoms. The developed approach should enhance the power of XPS for gaining information as such that is beyond the scope of conventional approaches.

1. Introduction

X-ray photoelectron spectroscopy (XPS) has been a powerful tool for the determination of the binding energy (BE) change of electrons in various orbits of a specimen upon chemical reaction or coordination environment change. Unlike the valence density-of-states (DOS) that provides direct information about charge repopulation and polarization during reaction,[1] the energy shift of a core level of an isolated atom gives profound information about the crystal binding energy that is dominated by the integrals of the specific eigen wave functions and the potentials of the interatomic binding and the intraatomic trapping. According to the band theory,[2] the intraatomic trapping determines intrinsically the specific energy level that changes with neither the crystal orientation or purity nor experimental conditions. However, the interatomic potential determines the core-level shift that is sensitive to the chemical and coordination environment.[2,3] The interatomic binding energy can thus be altered, but the intraatomic binding energy remains unperturbed as is for the isolated atom. Spontaneous processes such as bond nature alteration and bond length relaxation will affect the interatomic potential and hence shift the core level, intrinsically. The direction and the extent of the shift depend on the perturbation in the Hamiltonian of the sample.

Atoms at a free surface experience a local environment that is different from that of atoms in the bulk of a material. As a result, the energy associated with these undercoordinated atoms will, in general, be different from that of bulk atoms. In addition to the well-known chemical shift caused by the core-hole 'screening' due to charge transportation in reaction, the undercoordinated surface atoms can split the core band of a specimen into a few components,[3] according to their effective atomic coordination numbers (CN or z). However, definition of the number and the order of the components induced by surface relaxation remain quite controversial because of the lacking of guidelines for determining which peak arises from the surface and which one is from the bulk.

Intensive experimental evidence[4−13] shows that the intensity of the high-energy (small absolute value) component in an XPS spectrum often increases with the incident photon energy or with the decrease of the angle between the incident X-ray and the surface normal in the measurement. Speranza and Minati[14] clarified that by increasing the angle between the beam of photoelectrons and the surface normal of graphite from 0° to 85°, the X-ray penetration depth decreases from 8.7 to 0.7 nm. Dominated by the undercoordinated atoms, nanostructures exhibit that the core-level features move simultaneously toward lower BE when the size is reduced. It has been confirmed using XPS that the size induces a positive core-level shift of Ni,[15−17] Pt,[18−25] Au,[26−28] Cu,[29] Pd,[30] Si,[31] and carbon allotropes.[32−34] Obviously, increasing the incident photon energy or decreasing the emission angle will ensure more information from deep layers and vice versa; size reduction will increase the proportion of undercoordinated atoms of the nanostructures. Therefore, the trends of a surface core-level shift due to a change of incident photon energy and the emission angle and the trend of a nanosolid core-level shift due to the variation of the surface-to-volume ratio justify unambiguously that the undercoordinated atoms at a flat or at a curved surface dictate the surface- and size-induced positive BE shift.

With the widely used sign convention, a positive BE shift relates the low-energy (large absolute value) component to the surface contribution (S_i, $i = 1, 2, ..., B$) and the high-energy (small absolute value) component to the bulk origin (B). The resultant peak is often located in between the components and the exact position of the resultant peak varies with experimental conditions, which is perhaps why the documented values for the core-level energy of a specimen vary from source to source.

Although the BE of Ru(0001)[35] and Ru($10\bar{1}0$)[36] surfaces have been intensively investigated, the physical origin and the order

* To whom correspondence should be addressed. E-mail: ecqsun@ntu.edu.sg.
[†] Hunan University.
[‡] Nanyang Technological University.

10.1021/jp909549f
Published on Web 12/29/2009

and number of components of the 3d band remain to be clarified. Even more important is the information that we can exactly derive from the measurement. Here we show that consideration from the perspective of bond-potential−band correlation and its perturbation to the Hamiltonian is necessary. According to the band theory,[2] the core band shift is determined uniquely by the Hamiltonian if the specific eigen wave function is assumed to change insignificantly with the coordination environment. We also clarified that the BE should shift from the energy level of an isolated atom instead of from the bulk component in the XPS spectrum. Applying the tight binding approximation and the bond order−length−strength (BOLS) correlation mechanism,[3] we are able to derive quantitative information of the following, taking Ru $3d_{5/2}$ as an example for demonstration:

(i) The $3d_{5/2}$ energy level of an isolated Ru atom $E_{3d}(z = 0)$.

(ii) The BE shift of $\Delta E_{3d}(z = 12)$ from the $E_{3d}(z = 0)$ upon bulk formation.

(iii) The effective atomic coordination number z for the surface atomic layers.

(iv) A functional expression for the atomic-layer and crystal-orientation resolved energy shift.

(v) The z-dependence of the lattice strain, the binding energy density gain, and the atomic cohesive energy remnant in the surfaces up to skin depth.

(vi) More importantly, dominance of the perturbation of the Hamiltonian by the shorter and stronger bonds between undercoordinated atoms to the positive core-level shift.

2. Principle: Tight Binding Approach and BOLS Correlation

The coupling of the crystal potential, $V_{cry}(r, B)$, and the specific eigen wave functions determine the entire band structures of a bulk specimen (B, or $z = 12$) such as the band gap, the core-level shift, and the bandwidth, as well as the related properties such as dielectrics and electroaffinity according to the energy band theory.[2] The intraatomic trapping, $V_{atom}(r)$, determines the specific energy level of an isolated atom, from which the BE starts to shift upon interatomic interaction being involved. Under the equilibrium conditions of a bulk, the maximum value of $V_{cry}(r, B) = E_b$ is the cohesive energy per bond.

In the crystallite-imperfect regions such as at sites surrounding defects, adatoms, terrace edges, surfaces, and the skins of nanostructures, the single-body Hamiltonian is perturbed because of the bond strain and the associated bond energy gain that leads to the quantum trapping.[37] By introducing the perturbation coefficient, $\Delta_H = \gamma - 1$, the local single-body Hamiltonian becomes

$$H(\gamma) = \left[-\frac{\hbar^2\nabla^2}{2m} + V_{atom}(r)\right] + \gamma V_{cry}(r, B) \qquad (1)$$

The terms in the bracket correspond to the Hamiltonian of an electron moving around an isolated atom in the νth orbit. $V_{atom}(r)$ is the potential of intraatomic trapping that determines the νth energy level of an isolated atom, $E_\nu(z = 0) = \langle\phi_\nu(r_i)|V_{atom}(r)|\phi_\nu(r_i)\rangle$, from which the core level shifts when the crystal potential is involved. $\phi_\nu(r_i)$ is the specific Bloch wave function for the tightly binding core electron at site r_i, which satisfies $\langle\phi_\nu(r_i)|\phi_\nu(r_j)\rangle = \rho\delta_{ij}$, where δ_{ij} is the Kronecker δ function and ρ the charge density. According to the tight-binding approximation, the nonzero shift of a particular νth level, $\Delta E_\nu(z) = \gamma_z\Delta E_\nu(B) = \gamma_z(\beta + z\alpha) \propto \gamma E_b$, from the $E_\nu(0)$, is determined by the exchange β and the overlap α integrals.[3] Since the wave functions of the tight binding electrons in the inner shells are strongly localized, the α is much smaller than β. By forming the XPS bulk component whose maximal width is $2z\alpha$ ($10^{-(1\sim0)}$ eV level), one can estimate that the α is in the $10^{-(1\sim2)}$ eV order or even lower. The β is in the 10^0 eV level. Therefore, the BE shift is dominated by β, which is proportional to the cohesive energy per bond at equilibrium. The chemical bond, the potential well, and the core-level shift are thus strongly correlated.

According to the BOLS correlation, bonds between undercoordinated surface atoms are shorter and stronger. The interatomic potential well becomes deeper, and hence the energy levels of the undercoordinated atoms will go deeper accordingly. Because of the local bond strain, localized densification of charge, energy, and mass occurs to the sites of undercoordinated atoms. Thus, the broken-bond-induced local strain and quantum trapping provides perturbation to the Hamiltonian in the ith atomic site characterized by an effective atomic CN or z_i,

$$\begin{cases} \Delta_H = \Delta_i = \gamma_i - 1 = c_i^{-m} - 1 & \text{(Hamiltonian perturbation)} \\ c_i = 2/\{1 + \exp[(12 - z_i)/(8z_i)]\} & \text{(bond strain coefficient)} \\ c_i^{-m} = E_i/E_0 & \text{(potential well depth orbond energy gain)} \end{cases} \qquad (2)$$

The m is the bond nature indicator. For metals, $m = 1$. According to the band theory and the BOLS correlation, surface-induced energy shift of the νth level, $E_\nu(0)$, follows the relation:

$$E_\nu(i) - E_\nu(0) = \Delta E_\nu(B)(1 + \Delta_i) = [E_\nu(B) - E_\nu(0)]c_i^{-m} \qquad (3)$$

thus we have the relation,

$$\frac{E_\nu(i) - E_\nu(0)}{E_\nu(i') - E_\nu(0)} = \frac{1 + \Delta_i}{1 + \Delta_{i'}} = \frac{c_i^{-1}}{c_{i'}^{-1}} = \frac{c_{i'}}{c_i},\ (i' \neq i)$$

As the $E_\nu(0)$ is yet unknown, we need to take the bulk component as a reference, hence,

$$\frac{E_\nu(i) - E_\nu(B)}{E_\nu(i') - E_\nu(B)} = \frac{c_i^{-1} - 1}{c_{i'}^{-1} - 1},\ (i' \neq i) \qquad (4)$$

Given an XPS spectrum with clearly identified $E_\nu(i)$ and $E_\nu(B)$ components ($i = 1, 2, ...$), one can calculate easily the atomic $E_\nu(0)$ and the bulk $\Delta E_\nu(B)$ with the relations derived from eq 4:

$$\begin{cases} E_\nu(0) & = \dfrac{c_i E_\nu(i) - c_{i'} E_\nu(i')}{c_i - c_{i'}}, \qquad (i \neq i') \\ E_\nu(i) & = \langle E_\nu(0)\rangle \pm \sigma + \Delta E_\nu(B)c_i^{-1} \\ \Delta E_\nu(B) & = E_\nu(B) - \langle E_\nu(0)\rangle \end{cases} \qquad (5)$$

Equation 4 provides the constraint for decoding the surface core-level shift. If a total of l (>2) components are used to decompose a set of XPS spectra from differently oriented surfaces of a specific material, the $E_\nu(0)$ should take the mean value of the $N = C_l^2 = l!/[(l - 2)!2!]$ possible combinations with

a standard deviation of σ. The minimal σ serves as the criterion for the accuracy of spectral decomposition which involves the peak energies and the correspondingly effective CNs. The atomic CN is thus the unique parameter used for decomposition. One needs to note that the $E_\nu(0)$ and the $\Delta E_\nu(B)$ are intrinsic quantities that should not be affected by chemical, crystal, or experimental conditions. However, the change of crystal orientation leads to fluctuation of the effective atomic CNs of the specifically orientated surface layers and hence their corresponding component energies. The orientation change also affects the number of the components contributing to the spectral intensity, as the effective atomic CN may change slightly. Accuracy of the determination is subject strictly to the XPS data calibration.[38] Furnished with this approach to the XPS analysis, we would be able to elucidate the core-level positions of an isolated atom, the strength of bulk crystal binding, and the related properties, as discussed subsequently.

With the derived z_i and $E_\nu(i)$ for each surface component of fitting, we are able to predict the coordination-resolved local strain, core level shift (potential trap depth), binding energy density, and the cohesive energy per discrete atom in the surface skins:

$$\begin{cases} \varepsilon(z) = c_z - 1 & \text{(local strain)} \\ E_{3d}(z) - E_{3d}(0) = \Delta E_{3d}(12) c_z^{-1} & \text{(potential trap depth)} \\ E_d(z) = c_z^{-(m+3)} E_d(12) & \text{(binding energy density)} \\ E_c(z) = z_{ib} c_z^{-m} E_c(12) & \text{(atomic cohesive energy)} \end{cases} \quad (6)$$

where $z_{ib} = z/12$ is the reduced atomic CN, $z = 12$ is the standard bulk value, and $m = 1$ for the metal.

Hence, from the analysis of an XPS measurement, we are able to extract information such as bond order (z), length (d), strength (E_z), the ratio of binding energy density (c_z^{-4}), and the ratio of atomic cohesive energy ($z_{ib}c_z^{-1}$) in each of the Ru(0001) and Rh(10$\bar{1}$0) surface layers and sublayers. These quantities determine the surface properties and the process of catalytic reaction and growth nucleation.[37,39,40] For instance, the elastic modulus[39] is proportional to the binding energy density, and the melting point[37] is related to the atomic cohesive energy. More details regarding the interdependence of various physical and chemical properties have formed the subjects of two thematic reports on the size dependence of nanostructures and on the thermomechanical behavior of low-dimensional systems.[40,41]

3. Results and Discussion

On the basis of the developed approaches, we decode the XPS spectra by using Gaussian components with the constraint of eq 4 on the correlation between the component energies. The z values for the Ru surfaces are the initial input in optimization. The reason for using the Gaussian function instead of the Lorentz or the Doniach−Sunjic functions is that the Lorentz function is substantially the same as the Gaussian with modulated tails and the Doniach−Sunjic function is used for heavily asymmetric curves. From the first-order approximation, the Gaussian type deconvolution would be sufficient and simple, as demonstrated. In the deconvolution, the atomic CN for each sublayer is the only parameter that is adjustable.

Well-measured XPS profiles of the Ru(0001) and Ru(10$\bar{1}$0) surfaces were collected by the Lizzit[35] and Baraldi[36] groups using the super ESCA beamline of the ELETTRA synchrotron facility in Trieste, Italy. The experiments were carried out at

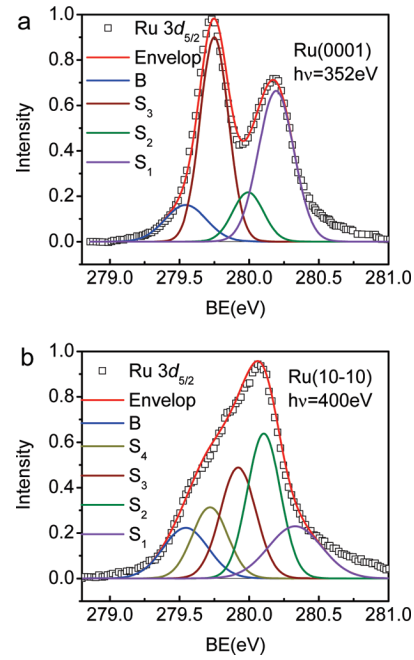

Figure 1. The decomposed XPS spectra for (a) the Ru(0001)[35] and (b) Ru(10$\bar{1}$0)[36] surfaces with derived information as summarized in Table 1. The Ru 3d$_{5/2}$ (279.544 eV eV) component remains identical for all orientations. (c) The CN-resolved potential trap depth represented by $E_{3d}(z) = \langle E_{3d}(0)\rangle \pm \sigma + \Delta E_{3d}(12)c_z^{-1} = 275.883 \pm 0.002 + 3.661/c_z$ (eV). The energy shift of each component is proportional to the magnitude of bond energy, which follows this relation: $\Delta E_\nu(i):\Delta E_\nu(12) = E_i:E_b = c_i^{-1}(i = S_1, S_2, ...)$.

130−270 K and an emission angle of 40° with an incident beam energy of 352−400 eV. The verification of experimental conditions just affects the overall intensity of the convoluted spectrum but not the energy position or width of each component. The two groups also decomposed the spectra. The number, peak width, and energy of components they optimized for each spectrum provide references for the current optimization and information extraction. The spectral low-energy tails in Figure 1 correspond to the quantum trapping of the even lower coordinated defect or edge atoms.

In order to ensure the minimal value of σ, fine-tuning of the z values was performed in the spectrum decomposition. The optimal results are shown in Table 1. The presently optimized z values for all the sublayers are identical to those derived from the same hcp surfaces of Be(0001), (10$\bar{1}$0), and (11$\bar{2}$0).[13,38] The well-defined BE shifts of Be surfaces allowed such z-value optimization,[13] which was used as a reference for the current iteration. The consistency of the effective CN for both the hcp Be and Ru surfaces amplify the reliability of this approach in determining the effective CN for the surface layers.

The $E_\nu(0)$ and $E_\nu(B)$ are intrinsic constants, which are identical for all the surfaces and subsurfaces of a given material, regardless of their orientations. For simplicity, we refer the energy shift of all surface components to the $E_\nu(B)$ before knowing the $E_\nu(0)$ value. Including the B component, there are a total of $l = 8$ components involved for the Ru(0001) and Ru(10$\bar{1}$0) surfaces, as shown in Figure 1. There is a combination of $C_8^2 = 8!/(8-2)!2! = 28$ $E_{3d}(0)$ values. Using the least-root-mean-square approach, we found the average $\langle E_{3d}(0)\rangle = \sum_N E_{3di}(0)/28 = 275.883$ eV with a standard deviation, $\sigma = \{\sum_{21}[E_{\nu i}(0) - \langle E_\nu(0)\rangle]^2/N/(N-1)\}^{1/2} = 0.0018-0.002$ eV. The bulk shift $\Delta E_{3d}(z = 12) = 3.661$ eV and the optimized $E_{3d}(B) = 279.544 \pm 0.002$ eV were thus obtained. The derived effective CNs, the local strains, and the predicted trends of the local binding

TABLE 1: Summary of the BOLS-Elucidated Information Regarding the Atomic-Layer- and Crystal-Orientation-Resolved Effective CN (z_i), Local Strain (c_i-1), and the Ratio of Binding Energy Density (c_i^{-4}) and Atomic Cohesive Energy ($z_{ib}c_i^{-1}$) Derived from the Measured XPS Profiles of Ru(0001)[35] and Ru(10$\bar{1}$0)[36] Surfaces under the Established Approach and the Constraints, Eq 4[a]

	i	$E_{1s}(i)-E_{1s}(B)$ (eV)	$E_{1s}(i)$ (eV)	z	c_z-1 (%)	E-density $[c_i^{-4}]$	$\Delta E_C(i)/E_c(B)$ $(z_{ib}c_i^{-1}-1)(\%)$
Ru	B	0	279.544	12.00	0.00	1.00	0.00
Ru(10$\bar{1}$0) ref 36	S_4	0.175	279.719	6.93	−4.57	1.21	−39.48
	S_3	0.377	279.921	4.80	−9.35	1.48	−55.88
	S_2	0.561	280.105	3.82	−13.30	1.77	−63.28
	S_1	0.785	280.329	3.11	−17.68	2.18	−68.52
Ru(0001) ref 35	S_3	0.205	279.749	6.48	−5.32	1.24	−42.97
	S_2	0.448	279.992	4.36	−10.91	1.59	−59.22
	S_1	0.649	280.193	3.50	−15.06	1.92	−65.66

[a] The least-mean-root-square method derives the $E_{1s}(0) = 275.883 \pm 0.002$ eV and the bulk shift $\Delta E_{1s}(12) = 3.661$ eV. The energy shift $E_{1s}(i)-E_{1s}(12)$ for each component is the input, and the effective CNs are the adjustable parameters. The B component ($z = 12$) at 279.544 ± 0.002 eV should be identical for all the surfaces of the same material.

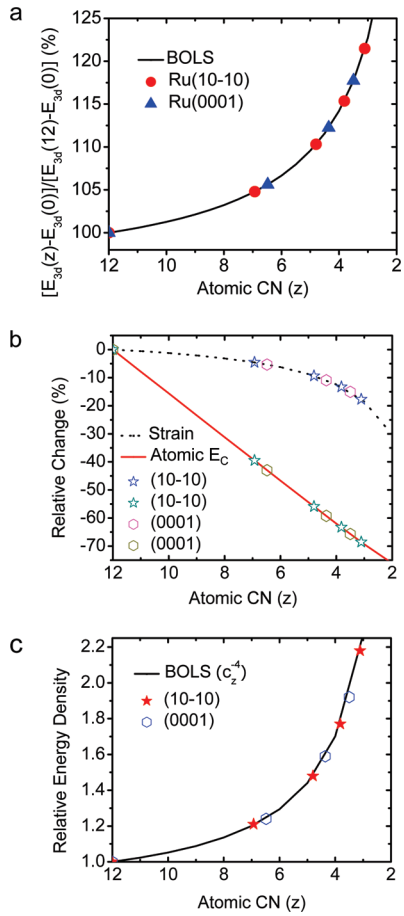

Figure 2. Comparison of the BOLS prediction with the derived CN (layer and orientation) − resolved (a) bond strain (%) and the relative change of atomic cohesive energy (E_C); (b) the relative energy density.

energy density gain and the atomic cohesive energy remnant are summarized in Table 1 and plotted in Figure 2.

Results show that the assignment of a positive core-level shift is more appropriate than the negative or the mixed shift assignment. The positive shift assignment, which is the consequence of Hamiltonian perturbation, allows us to derive the energy level of an isolated atom and its bulk shift as well as other demonstrated quantities. These quantities are of great importance in determining the surface properties and surface processes. The current derivatives favor more the mechanism of surface interlayer relaxation[4,8] than the "final-initial states" model; the latter model considered that no perturbation in the Hamiltonian should dominate. The photovoltaic effect and the excited final states may add artifacts to the XPS spectrum that could be removed by proper calibration in the measurement.[3] The CN-imperfection-induced bond strain and bond energy gain act on the core electrons at the energy levels of an atom whether it is in the neutral initial or the ionized final state. Therefore, joining the effect of CN-imperfection into the "initial-final states" model may make the modeling more comprehensive. Nevertheless, the developed approach has enabled us to elucidate quantitative information of the core-level position of an isolated atom and its shift due to bulk formation, as well as the quantitative information regarding the atomic-layer- and crystal-orientation-resolved effective atomic CN, local strain, binding energy density, and atomic cohesive energy, which is beyond the scope of a conventional approach using XPS or other techniques.

4. Conclusion

We have demonstrated a systematic analysis of the $3d_{5/2}$ BE shift of Ru(0001) and Ru(10$\bar{1}$0) surfaces, for instance, from the perspective of bond-potential-band correlation and Hamiltonian perturbation, which enabled us to elucidate the following information: (i) the $3d_{5/2}$ BE of an isolated Ru atom; (ii) the bulk shift of Ru $3d_{5/2}$; (iii) the effective atomic CNs and the corresponding local strains, and (iv) the trends of coordination-resolved binding energy density and cohesive energy in the surface and subsurface atomic layers. The developed approach could enhance the power of XPS for extracting more quantitative information regarding the surface process and properties. The concepts of local strain and quantum trapping are essential for understanding the bonding and electronic behavior of under-coordinated atoms in the surface and other atomic defect sites.

References and Notes

(1) Sun, C. Q. *Prog. Mater. Sci.* **2003**, *48*, 521.
(2) Omar, M. A. *Elementary Solid State Physics: Principles and Applications*; Addison-Wesley: New York, 1993.
(3) Sun, C. Q. *Phys. Rev. B* **2004**, *69*, 045105.
(4) Fang, B. S.; Lo, W. S.; Chien, T. S.; Leung, T. C.; Lue, C. Y.; Chan, C. T.; Ho, K. M. *Phys. Rev. B* **1994**, *50*, 11093.
(5) Alden, M.; Skriver, H. L.; Johansson, B. *Phys. Rev. Lett.* **1993**, *71*, 2449.
(6) Balamurugan, B.; Maruyama, T. *Appl. Phys. Lett.* **2006**, *89*, 033112.
(7) Navas, E.; Starke, K.; Laubschat, C.; Weschke, E.; Kaindl, G. *Phys. Rev. B* **1993**, *48*, 14753.
(8) Bartynski, R. A.; Heskett, D.; Garrison, K.; Watson, G.; Zehner, D. M.; Mei, W. N.; Tong, S. Y.; Pan, X. *J. Vac. Sci. Technol., A* **1989**, *7*, 1931.
(9) Andersen, J. N.; Hennig, D.; Lundgren, E.; Methfessel, M.; Nyholm, R.; Scheffler, M. *Phys. Rev. B* **1994**, *50*, 17525.
(10) Riffe, D. M.; Wertheim, G. K. *Phys. Rev. B* **1993**, *47*, 6672.

(11) Cho, J. H.; Kim, K. S.; Lee, S. H.; Kang, M. H.; Zhang, Z. Y. *Phys. Rev. B* **2000**, *61*, 9975.
(12) Fedorov, A. V.; Arenholz, E.; Starke, K.; Navas, E.; Baumgarten, L.; Laubschat, C.; Kaindl, G. *Phys. Rev. Lett.* **1994**, *73*, 601.
(13) Johansson, L. I.; Johansson, H. I. P.; Andersen, J. N.; Lundgren, E.; Nyholm, R. *Phys. Rev. Lett.* **1993**, *71*, 2453.
(14) Speranza, G.; Minati, L. *Surf. Sci.* **2006**, *600*, 4438.
(15) Matsui, F.; Matsushita, T.; Kato, Y.; Hashimoto, M.; Inaji, K.; Guo, F. Z.; Daimon, H. *Phys. Rev. Lett.* **2008**, *100*, 207201.
(16) Sun, Y.; Pan, J. S.; Tao, J. G.; Nie, Y. G.; Huan, C. H. A.; Zhang, Z.; Chai, J. W.; Li, D.; Wang, S. J.; Sun, C. Q. *J. Phys. Chem. C* **2009**, *113*, 10939.
(17) Tao, J. G.; Pan, J. S.; Huan, C. H. A.; Zhang, Z.; Sun, Y.; Chai, J. W.; Wang, S. J. *J. Phys.: Condens. Matter* **2008**, *20*, 485002.
(18) Lin, T. H.; Huang, T. P.; Liu, Y. L.; Yeh, C. C.; Lai, Y. H.; Hung, W. H. *Surf. Sci.* **2005**, *578*, 27.
(19) Sun, Y.; Wang, Y.; Pan, J. S.; Wang, L. L.; Sun, C. Q. *J. Chem. Phys. C* **2009**, *113*, 14696.
(20) Zhu, J. F.; Kinne, M.; Fuhrmann, T.; Denecke, R.; Steinruck, H. P. *Surf. Sci.* **2003**, *529*, 384.
(21) Yang, D. Q.; Sacher, E. *Chem. Mater.* **2006**, *18*, 1811.
(22) Bianchettin, L.; Baraldi, A.; de Gironcoli, S.; Vesselli, E.; Lizzit, S.; Petaccia, L.; Comelli, G.; Rosei, R. *J. Chem. Phys.* **2008**, *128*, 114706.
(23) Marcus, P.; Hinnen, C. *Surf. Sci.* **1997**, *392*, 134.
(24) Yang, D. Q.; Sacher, E. *J. Chem. Phys. C* **2008**, *112*, 4075.
(25) Bittencourt, C.; Hecq, M.; Felten, A.; Pireaux, J. J.; Ghijsen, J.; Felicissimo, M. P.; Rudolf, P.; Drube, W.; Ke, X.; Van Tendeloo, G. *Chem. Phys. Lett.* **2008**, *462*, 260.
(26) Ohgi, T.; Fujita, D. *Phys. Rev. B* **2002**, *66*, 115410.
(27) Howard, A.; Clark, D. N. S.; Mitchell, C. E. J.; Egdell, R. G.; Dhanak, V. R. *Surf. Sci.* **2002**, *518*, 210.
(28) Salmeron, M.; Ferrer, S.; Jazzar, M.; Somorjai, G. A. *Phys. Rev. B* **1983**, *28*, 1158.
(29) Yang, D. Q.; Sacher, E. *Appl. Surf. Sci.* **2002**, *195*, 187.
(30) Rao, C. N. R.; Kulkarni, G. U.; Thomas, P. J.; Edwards, P. P. *Chem.—Eur. J.* **2002**, *8*, 29.
(31) Sun, C. Q.; Pan, L. K.; Fu, Y. Q.; Tay, B. K.; Li, S. *J. Phys. Chem. B* **2003**, *107*, 5113.
(32) Sun, C. Q.; Sun, Y.; Nie, Y. G.; Wang, Y.; Pan, J. S.; Ouyang, G.; Pan, L. K.; Sun, Z. *J. Chem. Phys. C* **2009**, *113*, 16464.
(33) Kim, K. J.; Lee, H.; Choi, J. H.; Youn, Y. S.; Choi, J.; Kang, T. H.; Jung, M. C.; Shin, H. J.; Lee, H. J.; Kim, S.; Kim, B. *Adv. Mater.* **2008**, *20*, 3589.
(34) Hibino, H.; Kageshima, H.; Kotsugi, M.; Maeda, F.; Guo, F.-Z.; Watanabe, Y. *Phys. Rev. B* **2009**, *79*, 125431.
(35) Lizzit, S.; Baraldi, A.; Groso, A.; Reuter, K.; Ganduglia-Pirovano, M. V.; Stampl, C.; Scheffler, M.; Stichler, M.; Keller, C.; Wurth, W.; Menzel, D. *Phys. Rev. B* **2001**, *63*, 205419.
(36) Baraldi, A.; Lizzit, S.; Comelli, G.; Paolucci, G. *Phys. Rev. B* **2001**, *63*, 115410.
(37) Sun, C. Q.; Shi, Y.; Li, C. M.; Li, S.; Yeung, T. C. A. *Phys. Rev. B* **2006**, *73*, 075408.
(38) Sun, C. Q. *J. Phys. Chem. C* **2009**, *113*, in press.
(39) Liu, X. J.; Li, J. W.; Zhou, Z. F.; Yang, L. W.; Ma, Z. S.; Xie, G. F.; Pan, Y.; Sun, C. Q. *Appl. Phys. Lett.* **2009**, *94*, 131902.
(40) Sun, C. Q. *Prog. Mater. Sci.* **2009**, *54*, 179.
(41) Sun, C. Q. *Prog. Solid State Chem.* **2007**, *35*, 1.

JP909549F